World Scientific
www.worldscientific.com

Data-Driven Relationship for Reduction Factor of Ballasted Railway Bridge Deflections Due to Load Distribution Within Track

Reza Allahvirdizadeh [iD]*

Division of Structural Engineering and Bridges
KTH Royal Institute of Technology
Stockholm, Sweden
rezaal@kth.se

Emma Moliner [iD]

Department of Mechanical Engineering and Construction
Universitat Jaume I, Castellón, Spain

Pedro Museros [iD]

Department of Continuum Mechanics and Theory of Structures
Universitat Politécnica Valéncia, Valencia, Spain

Increasing the operating speed of the trains on modern networks necessitates performing dynamic analyses to assess the performance of bridges under passage of trains. The detailed investigation of their responses requires constructing complex computational models capable to take the train–track–bridge interaction effects into account. Such models have successfully been developed; however, employing those elaborated models for practical engineering applications, or to perform studies that require a large number of analyses may become infeasible. Among such situations are conducting probabilistic investigations, screening of entire networks, or sensitivity analyses. These concerns have been addressed by employing simplified models mostly relying on moving load modeling strategy which disregards the train–track–bridge interaction effects. Those neglected contributions can be compensated by implementing additional correction factors. The distribution of loads within track is one of those disregarded effects where a reduction factor is recommended by design guidelines to take its contribution into account. It has

*Corresponding author.

been shown that the existing relationship for these reduction factors delivers an acceptable performance for vertical accelerations, while showing a less favorable performance for displacements. Then, a data-driven strategy is adopted in this study to propose easy-to-apply relationships for reduction factors of deflections, due to load distribution within the track. In this context, three different distributive lengths of triangular load footprints have been considered, namely 2.0, 2.5 and 3.0 m. The procedure employed has trained and tested for more than 1 200 train configurations, comprising conventional, articulated and regular vehicles, and including several tens of thousand data points for each distributive length. The performance observed in the new models revealed a considerable improvement with respect to the existing relationship.

Keywords: Railway bridges; bridge dynamics; axle load distribution; data-driven modeling; track-bridge interaction; high-speed.

1. Introduction

Since the advent of the first high-speed rail transport in the world, the Japanese Shinkansen line connecting Tokyo and Osaka, there has been a continuous rise in demand for capacity on railway lines and their bridges. This implies not only an increase in operating speeds but also higher axle loads. Additionally, the commitment of modern societies toward achieving net-zero targets is pushing a modal shift of passengers and freight from road to more sustainable modes of transport. In this regard, railway will play a key role, with a reduced share of greenhouse gas emissions compared to road, marine or aviation transport.[1,2] The European Union (EU), in the framework of the recently launched *Sustainable and Smart Mobility Stategy*,[3] foresees that high-speed (HS) rail traffic will have doubled throughout Europe by 2030, and rail freight traffic by 2050.

The increase of railway capacity will require the upgrading of existing railway lines and the construction of new rail infrastructures. The interoperability, which is the capability of the railway system from different countries to operate together and enable safe and uninterrupted operation, has also become a prior goal in the EU to boost rail's performance and capacity toward the creation of a Single European Railway area. The European Union Agency for Railways (ERA) is responsible for the development of the Technical Specifications for Interoperability (TSI). Recently, ERA published a Technical Note on the investigations needed for closing TSI open points on railway bridge dynamics,[4] encouraging the improvement and revision of current simplified methods adopted in the regulations for the fast assessment of railway bridges under operating conditions.

Since the detection of ballast liquefaction in several simply-supported (S-S) bridges of the TGV high-speed line from Paris to Lyon, caused by excessive vertical vibrations, the European Committee for Standardization (CEN) limited the maximum admissible bridge deck acceleration to $3.5\,\mathrm{m/s^2}$ for ballasted tracks, constituting one of the most restrictive Serviceability Limit State (SLS) in the design of railway bridges as per EN 1990:2023.[5] Also this regulation prescribes strict requirements for the vertical deflections, among others.

An accurate prediction of the dynamic response of a railway bridge under traffic action requires a complex modeling,[6] since the problem addressed involves the interaction between four systems (the vehicle, the track, the bridge itself, and the soil on which it is built), and it is governed by a number of uncertain parameters.[7–10] Although the dynamic modeling has considerably evolved in recent years through the use of numerical models of increasing complexity for research purposes,[11–16] such advanced models demand high computational costs and may not be easy to implement in practice. They are useful or essential in a number of applications, as is the case of the development of *digital twins* for the detection of damage in Structural Health monitoring systems.[17–19]

However, the foreseen increase of railway lines capacity will require an evaluation of the condition of numerous bridges within the existing rail networks under new traffic requirements. Therefore, for preliminary assessments, sensitivity analysis or statistical screenings oriented to the identification of potentially critical structures in terms of vibrations, as a first step for subsequent research work, the computational cost plays a key role. Such computational effort is also crucial for the feasibility of probabilistic dynamic analyses, where large numbers of simulations are typically required.[20]

For this reason, a number of researchers have become involved in the development of closed-form solutions or straightforward numerical methods for a fast assessment of the dynamic compatibility between a large number of existing structures and new envisaged traffic conditions.[21–27] However, measures should be taken to prevent these simplified methods from resulting in an excessive overestimation of the bridge's response, as this could inaccurately jeopardize compliance with the serviceability limit states (SLS) specified in the current standards.

The simple and popular *moving loads model*, in which the train excitation is represented as a series of concentrated, constant-valued loads traveling at constant speed, has proven to be an efficient and quick strategy for a preliminary identification of critical parameters and vibration problems derived from an upgrading of the circulating conditions in existing railway bridges.[21] However, this approximation omits the beneficial effect that some interaction mechanisms may exert on the vibratory response of the bridge, as it is the case of the inertial effects of the train masses and the energy dissipation though the vehicle's suspension systems, or the distribution of the loads due to the presence of the sleepers and ballast layer,[28,29] among others. In order to take these effects into account in a straightforward manner, current regulations[30] have proposed simple formulas and reduction factors to be used in conjunction with the conservative moving load models. EN 1991-2[30] prescribes two simplified approaches to simulate the axle load spreading effect of the ballasted track in moving load models, by redistributing each axle load in (i) three consecutive sleepers (25%–50%–25%); or (ii) further distribution of the load from each sleeper to the deck through the ballast layer, following a 4:1 slope. Another

example is the *additional damping method* (ADM) from EN 1991-2, which approximated the vibration reduction associated to vehicle-bridge-interaction (VBI) to an additional amount of damping to be assigned to the bridge model. However, the ADM has been removed in the latest approved version of this regulation (EN 1991-2:2024[30]), due to its potential overestimation of the VBI benefit for particular combinations of the mechanical parameters of the train–bridge system.

The previous normative approaches were based on numerical studies performed by the committee of experts ERRI D-214, created by the European Rail Research Institute (ERRI) in 1995. Concerning the beneficial effect of the load distribution through the ballast, the final report of this committee (RP9,[31] also published as a UIC leaflet 776-2R[32]) provides a graph with two different reduction factors to be applied to the numerical results derived from moving load models. They correspond to the solution of a beam resting in an ideal elastic foundation, in which a footprint based on Zimmermann's solution[33] was considered as a distribution scheme for each axle load. The recommended reduction factors are associated to spread lengths of 2.5 m and 3.0 m, assuming different ballast depths. It is important to highlight that these studies were performed with the computational capabilities and the adequate model simplifications for that time.

Because the critical analysis and improvement of design methods is a matter of concern, a number of researchers are involved in this field. As it was mentioned before, some studies that questioned the ADM method[34,35] led to its elimination from the currently in force version of EN 1991-2[30] — which therefore does not contemplate the general use of VBI models for railway bridge analysis—, and new improved reduction factors to account for VBI effects are being proposed.[36] Also the beneficial effect of the load distribution through the ballast layer has been revisited by a number of researchers. Museros *et al.*[28] evaluated the effects of load distribution in the resonant acceleration response of beam bridges, considering a uniform spread of each point load over a length of 1 m. They observed that the shortest wavelengths $\lambda = V/f_1 \leq$ 4–5 m were more influenced by the distribution of the axle loads. Axelsson *et al.*[37] implemented a nonlinear finite element (FE) model of a ballasted track to quantify the load spread effect of the ballast through static analysis. They concluded that a simple triangular load distribution with a length of 3.0 m can be applied to each axle point load to represent the spread effect exerted by a ballast layer of 65 cm depth. Jin *et al.*[38] analyzed the load distribution phenomenon using analytical methods in the frequency domain. They demonstrated that the track acts as a low pass filter on the bridge acceleration levels. Based on this finding, they suggested a straightforward reduction factor for the bridge acceleration response predicted with moving load models, and presented a number of applications based also on triangular footprint distributions.

In a previous work of the authors,[39] a comprehensive, comparative study about the previously cited simplified methods to consider the beneficial effect of the

load-spreading exerted by the ballasted track was performed. Such comparative study revealed that, while the reduction coefficients proposed in the UIC leaflet 776-2R are correct to estimate the vertical accelerations, they are inadequate for the prediction of the bridge displacement response. Therefore, a novel data-driven reduction factor, suitable for the prediction of vertical displacement response of single-track, simple supported (S-S) railway bridges of short-to-medium span length, was proposed. The novel reduction factor was based on the spread effect generated by a triangular footprint scheme of 2.5 m length applied to each train axle load. According to the comparative study performed by the authors,[39] the intensity of distribution performed by a 2.5 triangle is intermediate, and analogous (in terms of accelerations) to the ERRI factor given in the UIC leaflet 776-2R for a spread length of 3.0 m — based on Zimmermann's solution.

Since the load distribution effect depends on the depth of the ballast layer, and this can be variable among different railway lines, for practical applications it is advisable to provide reduction factors for different intensities of the load distribution. Therefore, the purpose of this paper is to address the development of new data-driven reduction factors to predict the bridge vertical displacement response considering different realistic levels of the load spreading effect, aligned with existing codes of practice.[30,31] The new coefficients are based on the findings of the previous work from the authors,[39] whose results showed that triangular schemes of 2.0 m and 3.0 m length can be considered as practical lower and upper bounds of the distributive effect expected in ballasted tracks. The novel formulas proposed here aim to contribute to the development of safe and simplified methods for the preliminary assessment of SLS in short-to-medium S-S railway bridges, for which an increase of the circulating speed is envisaged. These simplified methods can be also exploited to take into account the load spreading effect in the framework of probabilistic dynamic analysis.

The strategy followed in this work does not take explicitly into account the track irregularities and track-wheel interaction. Considering those effects would imply the use of a complete vehicle–track–bridge interaction model, but the use of such detailed models — which probably will be necessary when analyzing particular bridges in depth — does not suit the reduced computational cost requirements justified earlier in this section. Therefore, the effects of track irregularities, in an approach as the one adopted here, must be considered *a posteriori* by means of corrective factors, such as for instance the coefficient φ'' adopted in Eurocode 1, following previous studies of the ERRI committee D-214.[31]

The paper is divided into the following sections: Section 2 describes the numerical approaches that are used throughout this work. Section 3 justifies the choice of the lower and upper bounds of the load distribution effect, represented through triangular footprint schemes of lengths 2.0 m and 3.0 m, respectively. In Sec. 4, the dataset created to train and develop the new data-driven reduction factors is

presented. It comprises single-track, S-S railway bridges of lengths in the range
4.8 m–25.2 m subjected to the passage of normative trains (HSLM-A model) along
with additional conventional and regular trains, and considering different distribu-
tive lengths for their axle loads. In Sec. 5, the data-driven formula for average spread
intensity developed by the authors in its previous work[39] is checked against the
previously created dataset. It is shown that new formulas are required to properly
estimate the reduction factors for displacements when lower and upper bounds of
distributive effects are to be considered. Section 6 explains the statistical treatment
and the methodology followed to develop the two new data-driven factors provided
in this work, and in Sec. 7, they are tested against 30% of samples of the original
dataset — which were randomly excluded to train the formula—, in addition to the
passage of an ensemble of real trains that were not considered previously. Finally,
Sec. 8 summarizes the main conclusions.

2. Numerical Modeling

In this work, the classical Simply-Supported (S-S), Bernoulli–Euler (B-E) beam
model has been adopted to idealize the bridge behavior. This constitutes a simple
and fast approach to evaluate the dynamic performance of beam-type structures in
which the inadmissible vibratory levels are mainly due to resonances of the funda-
mental mode, and has been widely used for preliminary serviceability checks under
traffic actions in practical applications.[21,22] As for the number of modal contribu-
tions, for the computation of vertical displacements, Pesterev *et al.* demonstrated
that the fundamental mode suffices to obtain practical results within engineering
accuracy.[40] Moreover, the authors showed in a previous work that the influence of
higher modes in S-S bridges diminishes markedly when load distributive schemes are
introduced.[39] Consequently, the evaluation of the vertical displacements are carried
out here by considering the vibrations of the first bending mode only.

Concerning the railway excitation, two simple alternatives that aligned with cur-
rent standards[30] are used in this research to generate a dataset of vertical vibratory
levels of beam bridges under traffic actions. First, the simple *moving loads model*
in which each axle of the train is considered as a moving concentrated load, is
adopted as a conservative reference scenario (Fig. 1(a)). It is well known that this
representation of the train excitation leads to conservative predictions of vertical

(a) Without load distribution.   (b) Triangular load distribution.
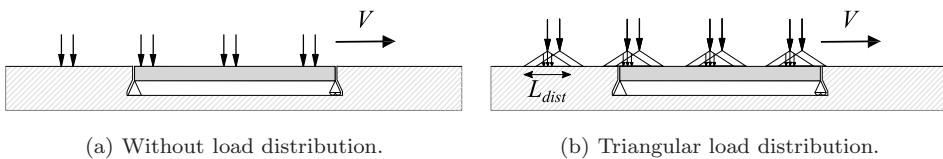
Fig. 1. Simplified numerical models.

bridge response because it neglects the distributive effect exerted by the ballasted track, especially for the shortest spans and wavelengths.[28] Second, the load spreading effect due to the presence of the sleepers and ballast is considered in this study by distributing each point load of the *moving loads model* through a triangular footprint scheme of equidistant loads spread over a certain distance L_{dist} (Fig. 1(b)).

As it was mentioned in the previous section, the use of a triangular distribution to smooth the intensity of each point axle load has proven to be a reasonable simplified strategy to represent the spread effect exerted by the ballasted track.[37–39] For this reason, in this work only this particular distribution is considered.

The simplified models shown in Fig. 1 are used in this work to compute analytically the maximum vertical deflection of a representative ensemble of beam bridges under the circulation of High Speed trains, in a wide range of speeds. These results will constitute the database. Therefore, the characteristics of the considered bridges to construct the dataset are described in Sec. 4.

3. Practical Limits of Distributive Length

For the intended proposed relationship to be suitable for practical applications, and with a view to cover the most usual analysis scenarios, reference values of the distributive length (L_{dist}) should be adopted.

It is well known that the intensity of the load distribution effect depends on the depth of the ballast layer. As regards the vertical displacements, such effect may be more or less pronounced, but will always be noticeable for the short wavelengths — and particularly for shorter bridges, as the authors have shown recently.[39]

However, the depth of the ballast layer can be variable among different bridges, and vary as well along the life span of a bridge. For those reasons, current European standards prescribe the use of two different values of bridge linear mass in dynamic analyses: a minimum value which is to be computed considering the lower expected thickness of ballast, and a maximum value in order to consider the possibility of future track lifts.[30]

Consistent with these facts, minimum and maximum values of L_{dist} associated to a ballasted track are adopted here. Regarding the definition of a minimum length, reference can be drawn from the most conservative distributive scheme considered in Eurocode 1[30]: such scheme contemplates that three consecutive sleepers receive load percentages 25%–50%–25% of each train axle force, respectively. Being enforced by current regulations, this three-sleeper scheme is often employed in engineering applications, and in applied research studies as well.[29] Previous studies from the authors have shown that the distributive effect of a triangular footprint of $L_{dist} = 2.0$ m is very similar to the reduction of the bridge response predicted by the aforementioned three-sleeper scheme.[39] Therefore, $L_{dist} = 2.0$ m is a convenient, practical lower bound of the distributive length that will be adopted in this study. The results obtained with $L_{dist} = 2.0$ m should be regarded as conservative, and such

distributive length may therefore be employed in analyses where upper bounds of the response are to be estimated.

As for the maximum value of L_{dist}, reference can be made to the work of Axelsson *et al.*,[37] where a significant ballast depth (0.65 m) is considered as an average of the thickness beneath sleepers in several Swedish bridges. In their study, which employs a nonlinear contact FEM model, Axelsson *et al.*[37] conclude that the effect of such ballast depth is well approximated by a triangular footprint of $L_{\text{dist}} = 3.0$ m. Therefore, such value will be adopted here as an upper bound of the distributive length. Since $L_{\text{dist}} = 3.0$ m will lead to a stronger prediction of the distributive effect, such value may be convenient for the analysis of existing bridges where concerns of dynamic behavior arise, providing that infrastructure managers effectively adopt a similar ballast depth in track maintenance.

Finally, an intermediate value $L_{\text{dist}} = 2.5$ m will deliver an averaged reduction effect between $L_{\text{dist}} = 2.0$ m and $L_{\text{dist}} = 3.0$ m. This feature can be convenient whenever screening studies are to be performed over wide ensembles of bridges/trains (similar to the recent papers from Grunert,[22] Reiterer *et al.*[25] or Museros *et al.*[23,41]), or for a tentative first assessment.

4. Dataset Generation

To the purposes of this paper, an extensive database is generated in this section based on the numerical modeling discussed in Sec. 2. For this objective, short to medium single span reinforced concrete bridges were analyzed under the following vehicles: 10 trains from the normative High Speed Load Model HSLM-A (articulated type) from EN 1991-2,[30] ensemble of conventional trains with distributed traction (Model 101, derived from Annex E in EN 1991-2,[30] see Museros *et al.*[42]), conventional trains with power cars (Model 103, derived from Annex E in EN 1991-2[42]) and regular trains (Model 303, derived from Annex E in EN 1991-2[42]).

The span length of the considered bridges varies in the range of 4.8 m and 25.2 m with a resolution of 1.2 m, which corresponds to twice the distance between two consecutive sleepers. A summary of their characteristics including span length, fundamental frequency, linear mass and damping ratio is reported in Table 1. It is worth pointing out that these characteristics are obtained by assuming slab bridges as the predominant reinforced concrete bridge type for shorter spans (i.e. bridges with $L < 15$ m) and voided concrete slab as the predominant bridge type for the longer bridges. A constant width of 5 m is assumed for slab bridges, while the width of voided concrete slab bridges is assumed to be 4 m plus 1 m length cantilever flanges. In addition, the diameter of the voids for bridges with voided concrete slabs is set at $0.6h$, where h is the deck thickness. The deck thickness (i.e. h) is calculated by fulfilling the maximum allowable vertical deflection and the lower limit for the bridge frequency prescribed in Refs. 5 and 30. In this context, the linear mass of the bridge is calculated by adding the concrete mass (assuming a constant mass density

Table 1. Characteristics of the considered bridges (L denotes the bridge span length, f_1 is their fundamental frequency, m is their linear mass and ζ denotes their damping ratio).

L (m)	f_1 (Hz)	m (kg/m)	ζ (%)
4.8	19.81	10 760	2.06
6.0	16.27	11 910	1.98
7.2	13.87	13 070	1.90
8.4	12.11	14 220	1.81
9.6	10.76	15 370	1.73
10.8	9.694	16 520	1.64
12.0	8.825	17 680	1.56
13.2	8.103	18 840	1.48
14.4	7.492	19 990	1.39
15.6	7.637	15 840	1.31
16.8	7.230	16 270	1.22
18.0	6.613	18 030	1.14
19.2	6.288	18 580	1.06
20.4	5.999	19 100	1.00
21.6	5.741	19 610	1.00
22.8	5.509	20 080	1.00
24.0	5.299	20 540	1.00
25.2	5.109	20 970	1.00

of $\rho_c = 2\,500\,\mathrm{kg/m^3}$) to that of the track and sidewalks. In addition, the modulus of elasticity of the concrete is set at $E_c = 35\,\mathrm{MPa}$, with a deduction of 10% for the reduction in stiffness due to cracking.

Then, as discussed in Sec. 3, each of these scenarios is analyzed under different load distribution cases including without any load distribution and also those with triangular load distributions with distributive lengths (L_{dist}) of 2.0, 2.5, and 3.0 m. The resonance and impact points are then selected as data points to be added to the dataset. However, it should be noted that load distribution causes some of those points to disappear in some of the cases which consequently caused those points to be disregarded. An example of such analyses along with the extracted data points for two different bridges and under passage of different trains is shown in Fig. 2.

Following this approach led to collect an extensive dataset with size of 2 41 771 for each of the considered distributive lengths (in total $2\,41\,771 \times 3 = 7\,25\,313$ data points). Then, this dataset is initially adopted to evaluate the accuracy of the existing relationships in this context and afterward it is used to develop a new relationship.

It should be mentioned here that the collected dataset is randomly partitioned into training dataset including the 70% of the samples and also the test set with remaining 30% of the data. The latter is used after termination of the training phase to evaluate the out-of-sample accuracy of the new trained models. In order to uniformly distribute all load models between training and test sets, the data points
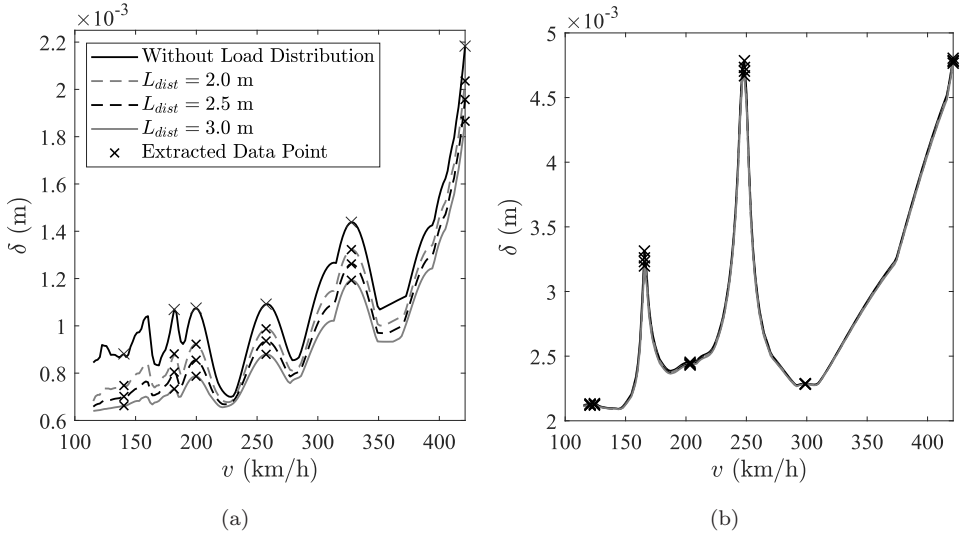
Fig. 2. Example of performed analyses to generate the dataset (δ denotes the maximum deflection of the bridge deck at each operating train speed of v). (a) Bridge with $L = 4.8$ m and under passage of HSLM-A1 load model, and (b) Bridge with $L = 25.2$ m and under passage of train #400 in load model 101.

corresponding to each load model are individually partitioned and then assembled to form the mentioned datasets.

As it can be seen in Fig. 2, the analyses are carried out starting at low speeds where no significant dynamic effect is expected in the bridges. Specifically, the minimum speed is selected to consider wavelengths down to 2.0 m, following the investigations of ERRI D-214.2 Committee.[43] As for the maximum speed, a value of 420 km/h is adopted, which is equal to a maximum circulation speed of 350 km/h increased by 20%, following the usual multiplicative factor adopted in European regulations for analysis with dynamic load models.[30]

5. Performance Evaluation of Existing Relationship

A data-driven relationship for reduction factors of deflections was proposed in Ref. 39 as Eq. (5.1). This relationship was developed for distributive length of 2.5 m, which was achieved using a limited training dataset including 31 data points which covers short to medium single-span reinforced concrete bridges. This relationship was proposed by first examining the correlation between the modeling parameters and the real reduction factors to determine the most important parameters to be implemented in the proposed relationship. The wavelength and the static amplification factor (i.e. the impact factor) were selected. The scatter plots of the real reduction factors versus the wavelengths of the collected dataset showed two clear

distinct regions of behavior when varying the reduction factor with respect to the wavelength. These two regions were then separated by selecting a threshold value for the wavelength using the K-Means clustering method. Then different types of relationships, including linear and polynomial equations in physical and logarithmic spaces, were investigated using iterative cross-validation techniques. In the case of polynomial equations, the best degree of parameters was determined using the cross-validation technique. Further details on the training procedure of Eq. (5.1) can be found in Ref. 39. The validity of this relationship was subsequently confirmed by performing a set of test analyses where a maximum error of 3.5% was reported.[39] Thus, the applicability of the existing equation for all considered distributive lengths is initially examined here using the extended dataset available in this study. It should be noted that the whole dataset is fed to the existing relationship at this stage:

$$\hat{\psi}_{2.5}(\boldsymbol{\theta}) = \begin{cases} \hat{\psi}_{2.5}^{(1)}(\boldsymbol{\theta}) = 0.55 + 0.58\theta_1 - 0.65\theta_2 - 0.19\theta_1^2 + 0.32\theta_1\theta_2, \\ \quad 2.0\,\text{m} \leq \lambda \leq 6.8\,\text{m}, \\ \hat{\psi}_{2.5}^{(2)}(\boldsymbol{\theta}) = \min\left[0.68 + 0.145\theta_1 - 0.026\theta_2, \quad 1.0\right], \\ \quad 6.8\,\text{m} < \lambda \leq 10\,\text{m}, \end{cases} \tag{5.1}$$

where $\theta_1 = \ln(\lambda)$ and $\theta_2 = \ln(\delta/\delta_s)$. Moreover, λ is the wavelength and δ/δ_s denotes the dynamic to static amplification factor (impact factor).

The relation between the true reduction factors (denoted here as $\psi_{2.5}$) and the estimated values using the existing equation (denoted here as $\hat{\psi}_{2.5}$) is presented in Fig. 3(a). An acceptable performance of the relationship is evident graphically. This is further examined by calculating the Root Mean Square Error (RMSE) according to Eq. (5.2). The RMSE estimates the average difference between the true and predicted values, which for data points with distributive length of 2.5 m is 0.015. It should be emphasized here that the RMSE has the same order of magnitude as the reduction factor, which illustrates the negligible deviation of the predicted reduction factors using the existing relationship from the true values in cases with distributive lengths of 2.5 m.

$$\text{RMSE} = \sqrt{\frac{1}{N}\sum_{i=1}^{N}(\psi - \hat{\psi})^2}, \tag{5.2}$$

where ψ denotes the true reduction factor, $\hat{\psi}$ is the reduction factor estimated by the proposed equation and N is the number of data points. In addition, the relative error measure is defined as Eq. (5.3) to evaluate the tendency of the existing relationship to under/overestimate the reduction factor values. The distribution of the relative frequency for cases with distributive length of 2.5 m is presented in Fig. 3(b). The skewness of the resulted distribution is -0.6, which shows that the existing relationship is almost symmetrical. In other words, it does not tend to underestimate

(a) Scatter plot true versus calculated.
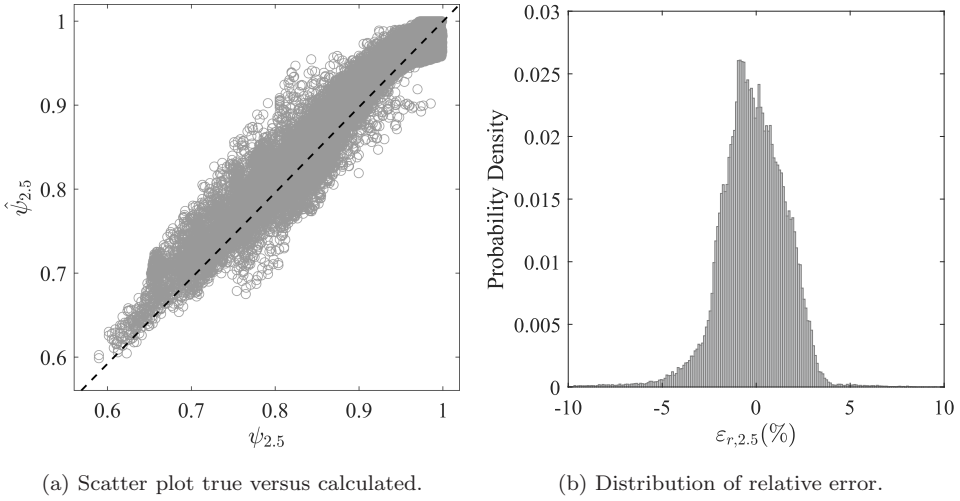
(b) Distribution of relative error.

Fig. 3. Relation between true reduction factors and the corresponding estimated values using Eq. (5.1) for data points with distributive length of 2.5 m.

or overestimate the reduction factor values. Moreover, the 99% Confidence Interval (CI) of the relative error distribution falls in the range of $[-6.7\%, 3.8\%]$ which is consistent with the conclusion drawn in Ref. 39. Therefore, the existing relationship appears to be accurate enough for cases with distributive length of 2.5 m:

$$\varepsilon_r = \frac{\psi - \hat{\psi}}{\psi} \times 100. \tag{5.3}$$

The other aspect that should be inspected is the continuity of the existing equation at the knot (point of separation between two parts of the equation). This aspect is investigated by varying the values for the impact factor in the range of $[1.0–10.0]$ and the wavelength close to the knot and evaluating the reduction factor based on the existing relationship. The variation of the results is presented in Fig. 4(a), which shows the discontinuity of the existing relationship. The amount of jump at the knot due to the discontinuity of the existing relationship is evaluated by the relative difference of the two parts of Eq. (5.1), i.e. $\hat{\psi}_{2.5}^{(1)}$ and $\hat{\psi}_{2.5}^{(2)}$. The relative difference estimates the normalized difference between the calculated reduction factors of $\hat{\psi}_{2.5}^{(1)}$ and $\hat{\psi}_{2.5}^{(2)}$ at the separating wavelength of these two parts of Eq. (5.1), i.e. $\lambda = 6.8$ m to the reduction factor calculated at this wavelength by $\hat{\psi}_{2.5}^{(1)}$. Since the proposed relationship depends not only on the wavelength but also on the impact factor (i.e. δ/δ_s), a range of impact factor values between $[1–10]$ is considered for the calculation of the relative difference. As can be seen in Fig. 4(b), the absolute value of the relative difference increases with the impact factor and reaches almost 2.0% for very large impact factor values. Therefore, the relative difference
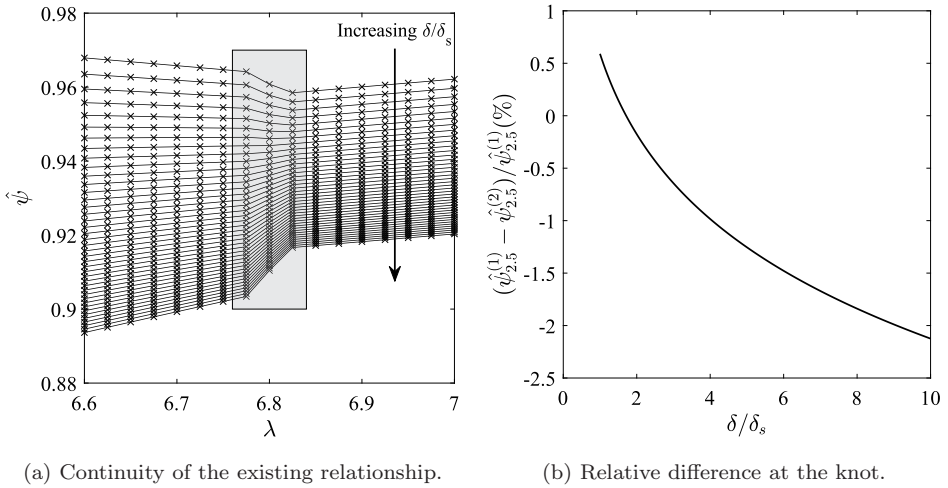
(a) Continuity of the existing relationship.

(b) Relative difference at the knot.

Fig. 4. Continuity of the existing relationship at the knot.

(a) Distributive length of 2.0 m.
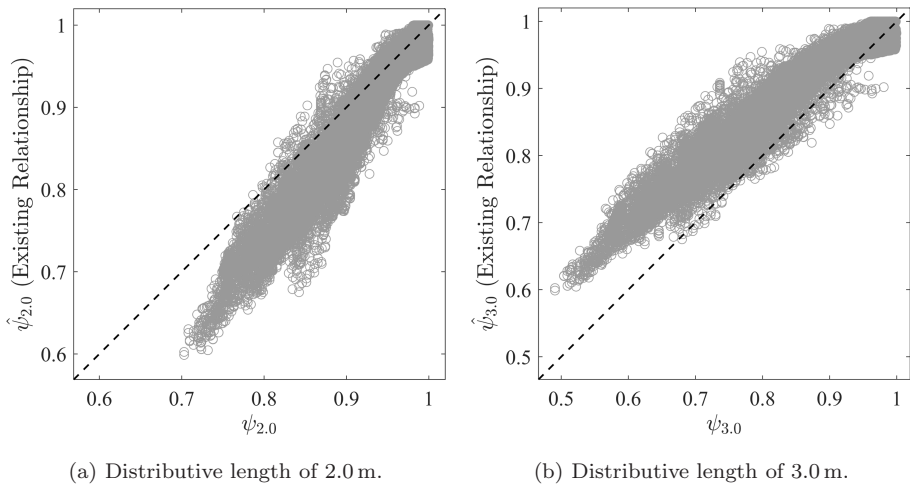
(b) Distributive length of 3.0 m.

Fig. 5. Performance of the existing relationship for reduction factor of displacements for other distributive lengths.

between the two parts of the existing relationship seems to be less than 2.0%. As a result, changing the existing relationship to account for the continuity condition seems unnecessary. In further estimations, an average value of the two parts of the relationship could be used to address this concern.

Subsequently, the performance of the existing relationship is evaluated here for other considered distributive lengths (i.e. 2.0 m and 3.0 m). For this purpose, the scatter plots of the true reduction factors are presented in comparison to the corresponding values estimated by the existing relationship (see Fig. 5). The poor

(a) Distributive length of 2.0 m.   (b) Distributive length of 3.0 m.
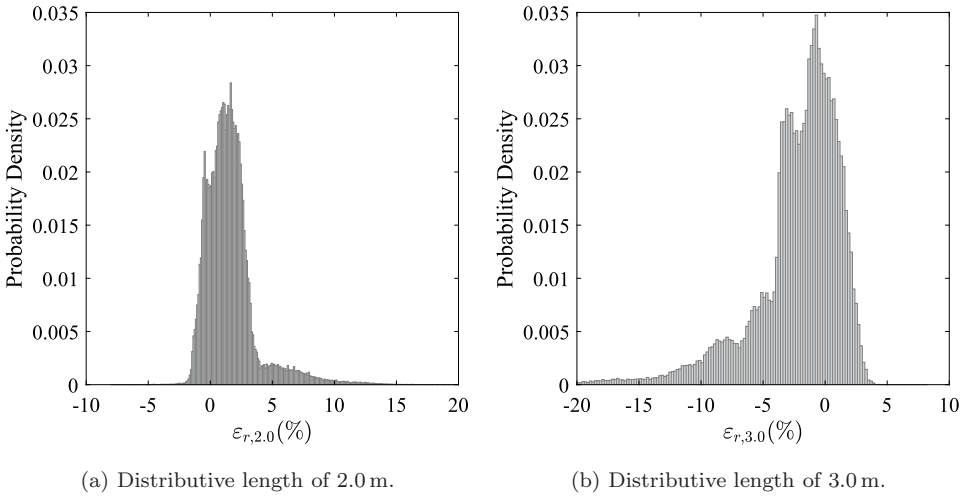
Fig. 6. The distribution of the relative error of the existing relationship for reduction factor of displacements with respect to other distributive lengths.

performance of the existing relationship is obvious. As can be seen (and as was expected), it tends to overestimate the reductions for shorter distributive lengths (i.e. distributive length of 2.0 m) and underestimate those for longer distributive lengths (i.e. distributive length of 3.0 m). Therefore, the previously proposed relationship cannot be adopted for such situations without further adjustments.

The tendency of the existing relationship to underestimate or overestimate the reduction factor for other distributive lengths is further assessed using the relative error measure (Eq. (5.3)). The distributions of the relative error of the existing relationship with respect to these distributive lengths are shown in Fig. 6. The skewness of the distribution for distributive lengths of 2.0 m and 3.0 m is estimated as 2.06 and −1.80, respectively. The high positive and negative values highlight the tendency of Eq. (5.1) to overestimate (right-tailed) or underestimate (left-tailed) the reduction factor for distributive lengths of 2.0 m and 3.0 m, respectively. In this context, the 99% CI of the relative error distribution for the distributive length of 2.0 m is [−1.5%–11.4%], while the 99% CI for the distributive length of 3.0 m varies in the range of [−18.4%–3.0%]. These discussions highlight the necessity of proposing new relationships to estimate the reduction factor of displacements for cases with other distributive lengths.

6. New Data-Driven Relationship

Regardless of which distributive length is adopted, the performed analyses would be carried out in linear regimes. This could result in the estimated responses being linearly correlated when using different load distribution schemes. Since the existing

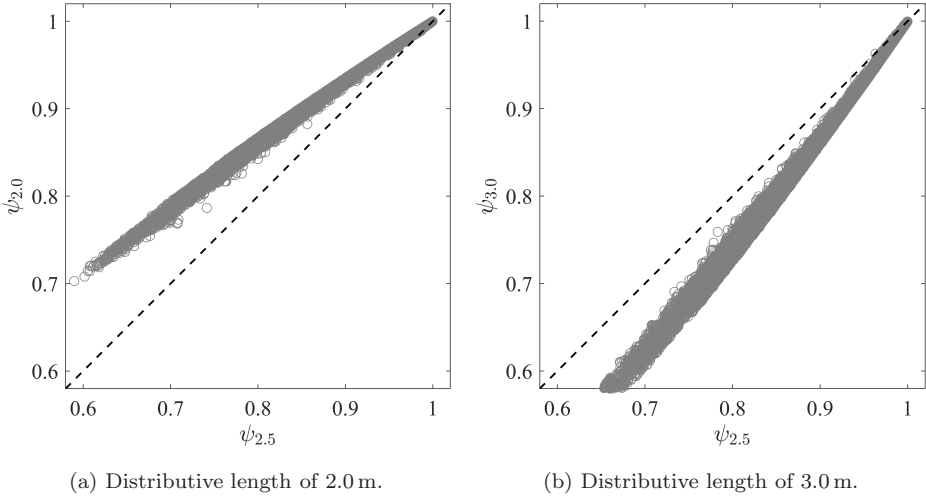(a) Distributive length of 2.0 m. (b) Distributive length of 3.0 m.

Fig. 7. The correlation between reduction factor of the other distributive lengths with those corresponding to the distributive length of 2.5 m.

relationship appears to be accurate enough for the reduction factors of cases with distributive lengths of 2.5 m, the possibility of adjusting this relationship for other situations is initially investigated here. The possibility of proposing alternative formulations is considered if such adjustments would not be satisfactorily accurate. It should be mentioned here that the discussions in this section are conducted using a randomly selected training dataset. This comprises 70% of the entire dataset and the remainder is used to test the proposed relationships. Furthermore, the randomly partitioned datasets contain a uniform distribution of all train types and also all considered bridges.

The correlation between true values of the reduction factor in cases with other distributive lengths and those corresponding to the distributive length of 2.5 m is presented in Fig. 7. A very linear correlation is evident between these cases. Therefore, it seems possible to model the reduction factor using other distributive lengths based on the existing model for distributive length of 2.5 m, which can be formulated as Eq. (6.1).

$$\hat{\psi}_{L_{\text{dist}}}(\boldsymbol{\theta}) = f_{L_{\text{dist}}}(\hat{\psi}_{2.5}(\boldsymbol{\theta})), \tag{6.1}$$

where $f_{L_{\text{dist}}}(\cdot)$ is the mapping function that transforms the estimated reduction factor using Eq. (5.1) to the desired distributive length.

The observed linear correlation encourages to consider straightforward polynomial functions with first and second degrees as potential candidates for such transformation functions. These polynomial functions are applied in both natural and logarithmic spaces. Taking this into account, a cross-validation technique is

applied to select the proper model type among these potential mapping functions. The procedure is repeated 100 times and the model with the smallest median and standard deviation error measure is selected.

At this stage, a Weighted Root Mean Square Error (WRMSE) as Eq. (6.2) is used as the error measure. The reason for this is that the smaller the reduction factor is, the more important it is for the estimated response of the bridge. Therefore, accurate prediction of the data points with a smaller reduction factor would be more important than those closer to 1.0. It is also important that the relationship developed is more on the safe (conservative) side. In other words, greater weight should be given to cases where the predicted reduction factor is smaller than the true value. In view of this, a weighting function such as Eq. (6.3) is used in this study.

$$\text{WRMSE} = \sqrt{\frac{\sum_{i=1}^{N} w_i (\psi - \hat{\psi})^2}{\sum_{i=1}^{N} w_i}}, \tag{6.2}$$

where w_i is the weight of each data point as Eq. (6.3).

$$w(\psi, \hat{\psi}) = \eta_1 \text{h}(\psi - \hat{\psi}) \exp(\eta_2 \psi + \eta_3) + \text{h}(\hat{\psi} - \psi) \exp(\eta_2 \psi + \eta_3), \tag{6.3}$$

where η_1 assigns a higher importance to cases in which the trained model is not conservative, i.e. the predicted reduction factor is smaller than the true value ($\psi > \hat{\psi}$). Moreover, η_2 and η_3 define the shape of the weight function depending on the true value of the reduction factor. It is assumed that the true reduction factor varies between 0.5 and 1.0, which leads to $\eta_2 = -\eta_3$.

To determine these parameters, a grid-search optimization is performed here. Only 10% of the dataset is adopted for this objective. The reason for this is that using the entire dataset can increase the possibility of training over-fitted models. The contour plots of the objective function of the above optimization as a function of η_1 and η_2 are shown in Fig. 8. It is worth noting that the objective function of tuning these parameters is defined as the multiplication of the absolute skewness of the relative error of the best trained model in the width of its 99% CI and WRMSE. The scales of these measures are different; therefore, they are each transformed into a uniform scale. In this way, $\eta_1 = 1.35$ and $\eta_2 = -3.22$ are obtained for the cases with distributive length of 2.0 m. Similarly, $\eta_1 = 1.65$ and $\eta_2 = -3.22$ are obtained for the cases with distributive length of 3.0 m. The shape of the assigned weights would therefore be as shown in Fig. 9.

Following the approaches described above, the variation of the cross-validated WRMSEs of the considered mapping functions under consideration is shown in Fig. 10 for both distributive lengths. As can be seen, quadratic polynomial mapping functions in natural space presents a better performance both from the point of view of accuracy and stability compared to the other function types. This statement seems to be true for both considered distributive lengths.

(a) Distributive length of 2.0 m.   (b) Distributive length of 3.0 m.
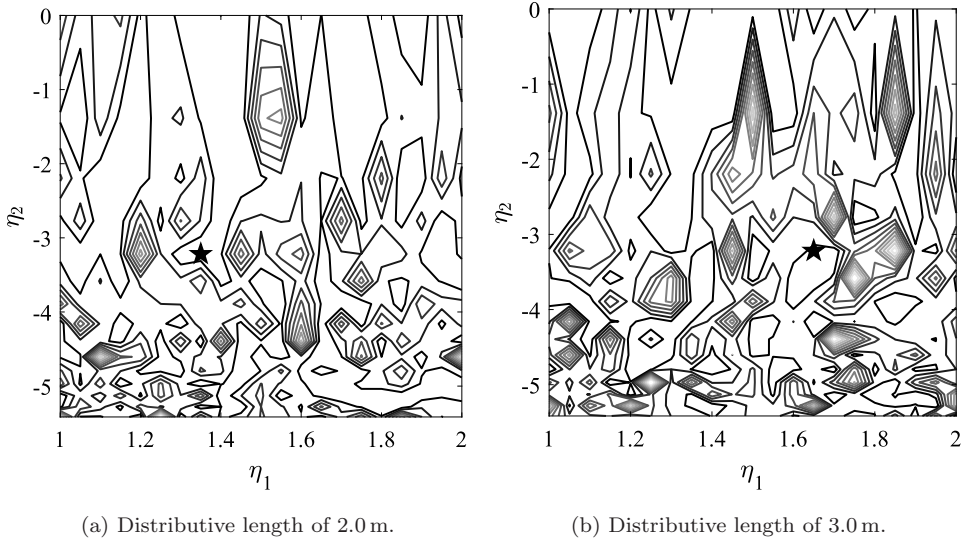
Fig. 8. Tuning the parameters of the WRMSE (the star point presents the combination of parameters minimizing the objective function).
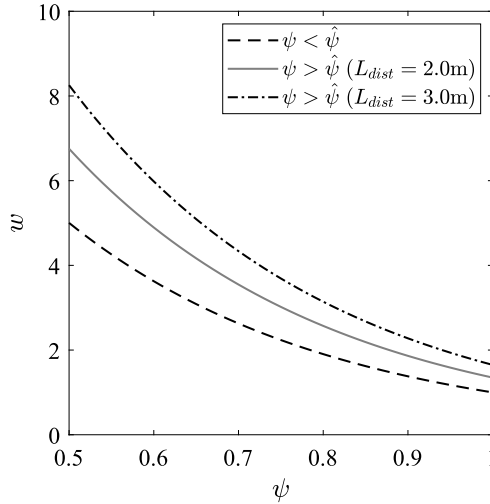

Fig. 9. The shape of the assigned weight used in WRMSE.

The reduction factor of the experienced displacements by the bridge due to the load distribution within the track for different distributive lengths can therefore be formulated as Eq. (6.4). The parameters of the new relationship for the reduction factor as well as the relation for cases with distributive length of 2.5 m are similar to

(a) Distributive length of 2.0 m.

(b) Distributive length of 3.0 m.
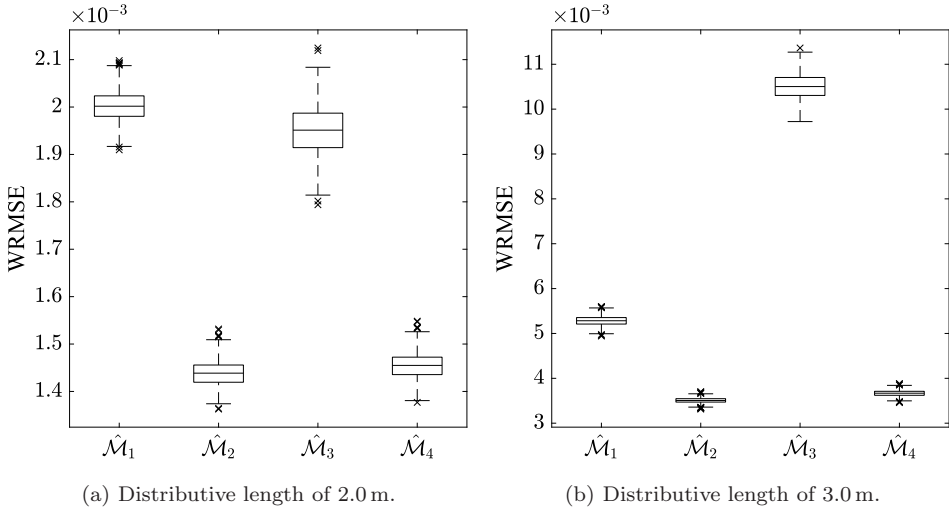
Fig. 10. The variation of WRMSE using cross-validation technique to select the best mapping function for other distributive lengths ($\hat{\mathcal{M}}_i, i = 1, \ldots, 4$ correspond to the first- and second-degree polynomial functions with input parameter — reduction factor of cases with distributive length of 2.5 m — in natural and logarithmic spaces).

the existing relationship (see Eq. (5.1)). To estimate the reduction factor for cases with distributive lengths other than 2.5 m, the existing relationship is first used to calculate the reduction factor corresponding to distributive length of 2.5 m and then it is mapped to the other distributive lengths:

$$\hat{\psi}(\boldsymbol{\theta}) = \begin{cases} 0.12 + 1.1\hat{\psi}_{2.5}(\boldsymbol{\theta}) - 0.23(\hat{\psi}_{2.5}(\boldsymbol{\theta}))^2, & L_{\text{dist}} = 2.0\,\text{m}, \\ \hat{\psi}_{2.5}(\boldsymbol{\theta}), & L_{\text{dist}} = 2.5\,\text{m}, \\ 0.13 + 0.32\hat{\psi}_{2.5}(\boldsymbol{\theta}) + 0.55(\hat{\psi}_{2.5}(\boldsymbol{\theta}))^2, & L_{\text{dist}} = 3.0\,\text{m}. \end{cases} \qquad (6.4)$$

A final improvement is implemented to take into account the feedback obtained when testing the new proposed relationship. During the application of Eq. (6.4) to other types of real trains — not included in the database used to train the proposed formula (see Sec. 7.2)—, it was found that there was a slight deviation at the shortest wavelengths ($\lambda < 2.8$ m). The reason behind the deviation is the scarce number of resonant peaks present in that low-response region, which makes the proposed formula less capable of capturing with accuracy the behavior for the shortest wavelengths.

To deal with this situation, a linear correction to Eq. (5.1) in the range 2.0 m < $\lambda < 2.8$ m has proved convenient, leading to the following final expression to be

used in conjunction with Eq. (6.4):

$$\hat{\psi}_{2.5}(\boldsymbol{\theta}) = \begin{cases} \max\left[(1.358 - 0.128\lambda), 1.0\right] \times \hat{\psi}_{2.5}^{(1)}(\boldsymbol{\theta}), & 2.0\,\mathrm{m} \le \lambda \le 6.8\,\mathrm{m}, \\ \hat{\psi}_{2.5}^{(2)}, & 6.8\,\mathrm{m} < \lambda \le 10\,\mathrm{m}. \end{cases} \tag{6.5}$$

7. Test the New Relationship

This section is dedicated to evaluating the performance of the proposed relationship. It is achieved by following two approaches. First, the test set is used, i.e. 30% of the entire dataset that the models have not seen during the training phase. Then, some particular train types that were not included in the original dataset are employed performing full dynamic analyses. In this context, the outcomes of the model with explicit track consideration are compared with those resulting from the application of the proposed reduction factor without modeling the track.

7.1. *Validation within the dataset*

The scatter plots of the predicted reduction factors using the proposed relationship compared to the true values are presented in Figs. 11(a) and 12(a) for cases with distributive lengths of 2.0 m and 3.0 m, respectively. It is evident that the trained models are capable to predict the general trend of the true values, which means that they can be considered as unbiased models. It can be well understood by comparing these performances with those observed in Fig. 7. It is recalled that 30% of the entire dataset which the models have not seen during the training phase is used for this validation.

(a) Scatter plot true versus calculated.   (b) Distribution of the relative error.
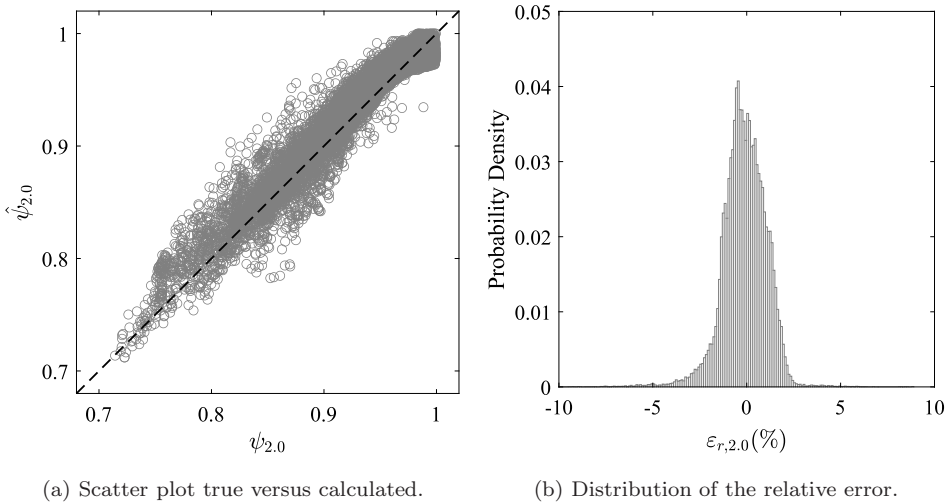
Fig. 11. The relation between true reduction factors and the corresponding estimated values using new trained model for cases with distributive length of 2.0 m.
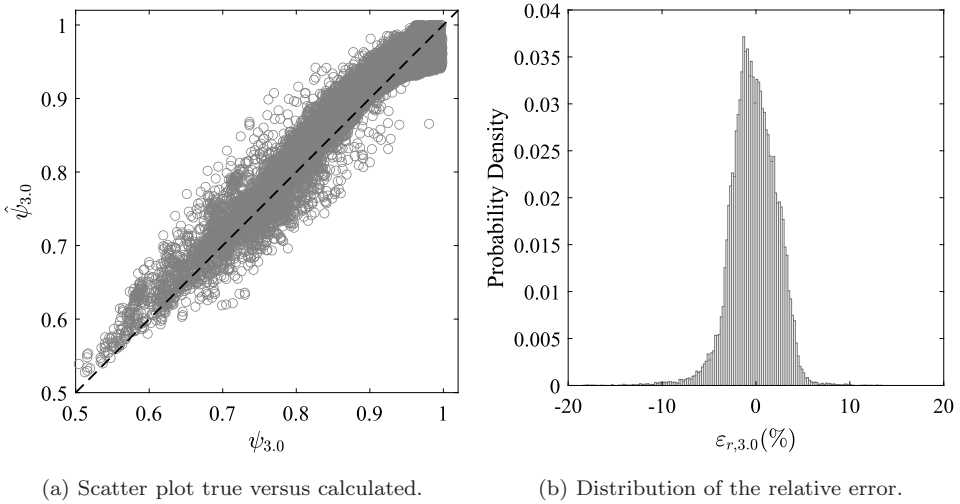
(a) Scatter plot true versus calculated.

(b) Distribution of the relative error.

Fig. 12. The relation between true reduction factors and the corresponding estimated values using new trained model for cases with distributive length of 3.0 m.

The accuracy of the proposed relationship is further evaluated by considering the distribution of the relative error, as shown in Figs. 11(b) and 12(b) for cases with distributive lengths of 2.0 m and 3.0 m, respectively. The skewness of the distribution of the relative error is obtained as -0.67 and -0.49, which confirms that the trained models do not tend to overestimate or underestimate the reduction factor. The 99% CI of the relative error for cases with distributive length of 2.0 m resulted as $[-4.7\%$–$2.6\%]$. In other words, the maximum error of the trained models for these cases would most probably be less than 5.0%. Similarly, the 99% CI of the relative error for cases with distributive length of 3.0 m resulted as $[-8.9\%$–$5.4\%]$. In this case, a lower accuracy is observed as the maximum error is most likely below 9.0%; however, a significant improvement over the existing relationship is evident.

7.2. *Validation under actual rolling stock*

Next, the proposed formulas have been checked against the passage of 10 additional real trains that were not included in the database. In particular, the following vehicles have been used: ICE-4 high-speed train,[44] the Steel Arrow train that is used for steel ore transports in northern parts of Sweden,[45] the Chinese Pioneer train,[46] the passenger train Railjet that operates in high-speed lines from Austria,[29] the Portuguese Alfa Pendular train,[47] the Spanish high-speed composition Renfe S-100,[25] the high-speed Thalys train in both single and double formation[48] (i.e. with two intermediate power cars), and finally the Spanish Renfe S-102 of regular type which also circulates in single and double formations.[49]

The maximum vertical displacement response of all considered bridges in this study (i.e. the bridges with the characteristics given in Table 1), under the circulation of the 10 real trains in a speed range $V = [v_{\min}, 420]$ km/h in 1.8 km/h steps, has been computed using the numerical models with triangular load distribution and distributive lengths of $L_{\text{dist}} = [2.0, 2.5, 3.0]$ m (see Fig. 1(b)), and also by using the three data-driven formulas proposed in this work (i.e. Eqs. (6.4) and (6.5)). Although the maximum circulating speeds of the real trains are actually different, for validation purposes the same maximum speed has been considered for all of them. The speed $v_{\min}$ is selected in each case to consider a minimum wavelength of 2.0 m, following the approach presented in Sec. 4.

The relative error between the real (δ) and estimated ($\hat{\delta}$) resonant displacements under the passage of the ten trains has been estimated as per Eq. (5.3) in all the span lengths. Figure 13 collects the maximum positive and negative relative errors for each span and circulating train, for the lower and upper bounds of the distributive lengths (2.0 m and 3.0 m). The results are plotted versus the span length, and a different marker is assigned to each train.

In general terms, it can be observed that the results associated to the distributive length of 3.0 m lead to slightly higher errors than those obtained for the lowest intensity of the load spread effect. The distribution $L_{\text{dist}} = 2.5$ m, which is not shown in the plot for conciseness, exhibits similar trends and error thresholds. The maximum positive errors (meaning that the data-driven formula is non-conservative) are kept below 6% in the prediction of the resonant response. The maximum negative errors are somewhat higher, but mainly kept below 10%, with the exception of a number of particular train passages across the shortest span lengths, considering a
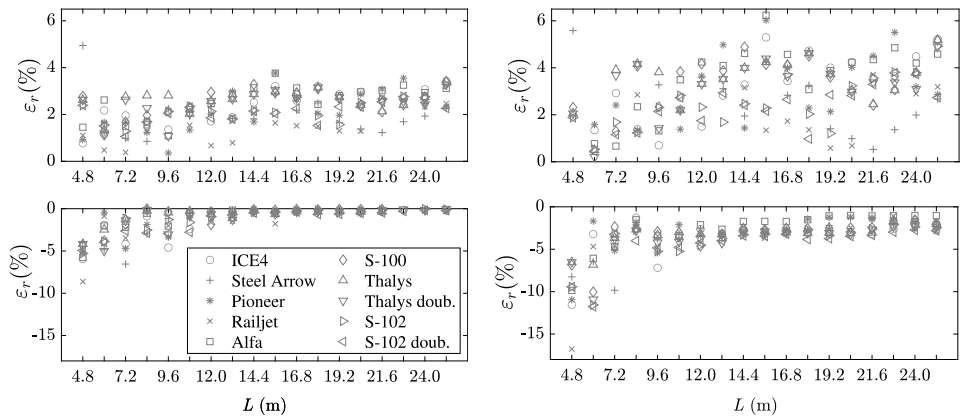
(a) Distributive length of 2.0 m. (b) Distributive length of 3.0 m.

Fig. 13. Relative errors between true and estimated resonant displacements.
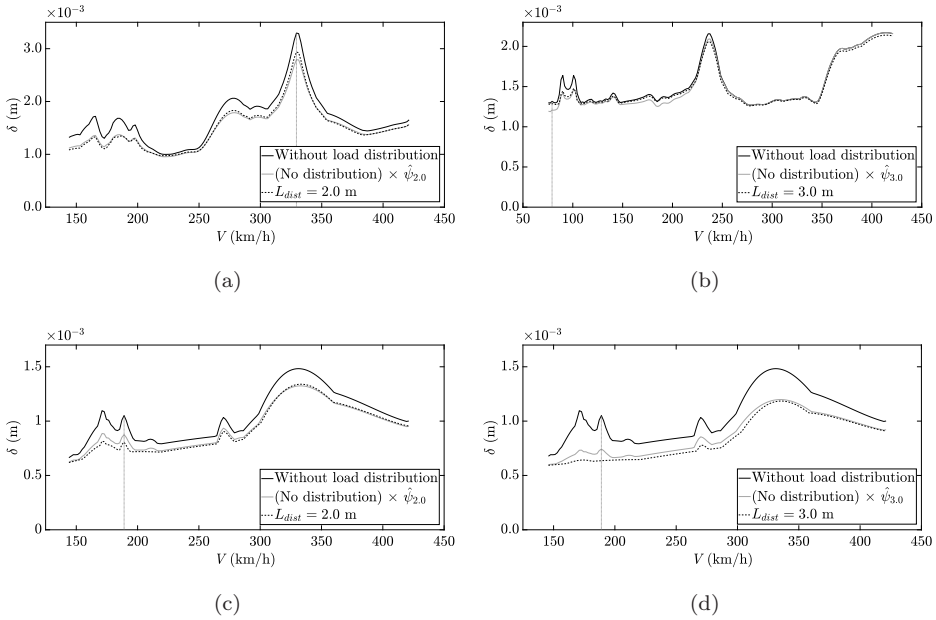
Fig. 14. Envelopes of vertical displacement for the cases leading the highest relative errors. (a) $L = 4.8$ m under the passage of Steel Arrow, (b) $L = 16.8$ m under the passage of Alfa Pendular train, (c) $L = 4.8$ m under the passage of Railjet, and (d) $L = 4.8$ m under the passage of Railjet.

high intensity of the load distribution (Fig. 13(b)). This implies that in a limited number of cases, the new proposed formulas are slightly conservative.

For a better understanding and interpretation of the previous relative errors, in the next figure the displacement response in those cases leading to the highest positive and negative errors is analyzed. Figures 14(a) and 14(c) collect the stronger deviations associated to the distributive length of 2.0 m. A maximum positive error of 5% has been measured in a resonant peak induced by the passage of the Steel Arrow train at a speed of 330 km/h, which is marked in the top figure with a vertical dotted line. It also should be mentioned that the maximum circulating speed of this train is around 160 km/h. The maximum negative error is also marked in Fig. 14(c), and corresponds to the passage of the train Railjet at 189 km/h. In this case, the relative error attains −8.5%. Despite the fact that the data-driven formula is slightly conservative, the reduction of both peak responses below 200 km/h with respect to the moving loads model is very noticeable, meaning that the reduction effect due to the ballasted track is largely captured by the proposed relationship.

Figures 14(b) and 14(d) illustrate the worst scenarios for the distributive length of 3.0 m. The maximum positive error, meaning that the developed formula is non-conservative, takes place in the span length of 16.8 m under the circulation of the Alfa Pendular train. Although the maximum relative error attains 6%, it can be seen
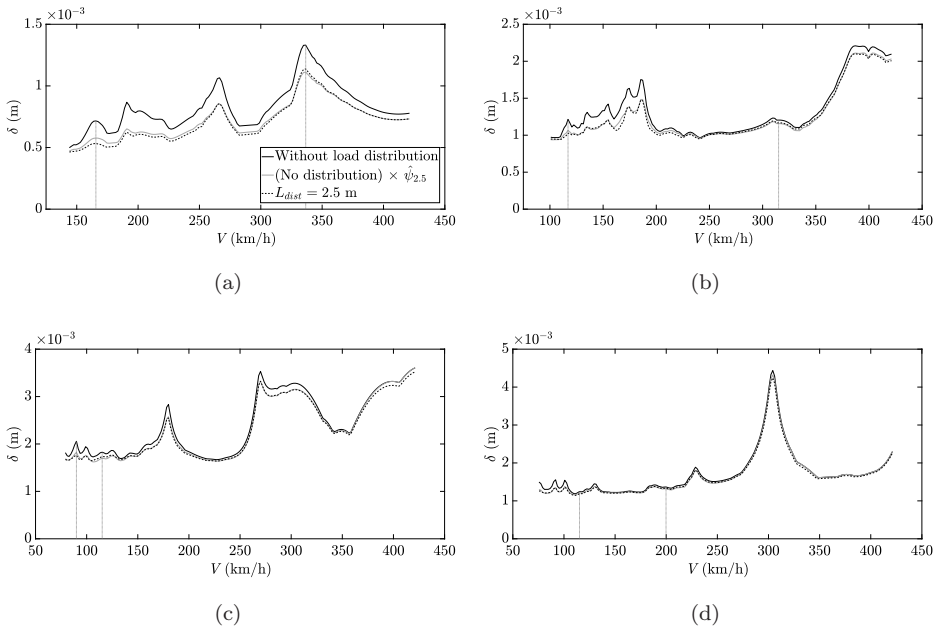
Fig. 15. Envelopes of vertical displacement for a distributive length of 2.5 m. Legend applies to all subplots. (a) $L = 4.8$ m with train Renfe S-100, (b) $L = 7.2$ m with Thalys (double), (c) $L = 9.6$ m with Steel Arrow train, and (d) $L = 12.0$ m under the passage of ICE-4.

that it takes place at a low speed (79.2 km/h) in which the contribution of the quasi static response prevails in the response, and is not relevant for the verification of the limit states in practical applications. Again, the resonant peaks below 200 km/h for the 4.8 m bridge are largely smoothed out.

Additional displacement responses are plotted in Fig. 15 for the distributive length of 2.5 m. Span lengths and train passages different from those shown previously are presented. In each subplot two vertical dotted lines represent the maximum positive and negative relative errors found in the resonant response for the range of speeds considered. As can be seen, the data-driven formula approaches well the beneficial effect of the load distribution even in the non-resonant range. It is also noticeable in this figure how the reduction of response derived from the load spreading decreases drastically as the span length increases (see for instance Figs. 15(a) and 15(d)).

For the sake of completeness, Fig. 16 shows additional train passages over the span of 6.0 m length, in which the spread effect is significant. Again, the maximum and minimum relative errors found in the resonant peaks are marked with vertical dashed lines. Two different load distributions are compared: the lower bound $L_{\text{dist}} = 2.0$ m in Figs. 16(a) and 16(c); and the upper bound $L_{\text{dist}} = 3.0$ m in Figs. 15(b) and 15(d). The correspondence between the numerical predictions considering the
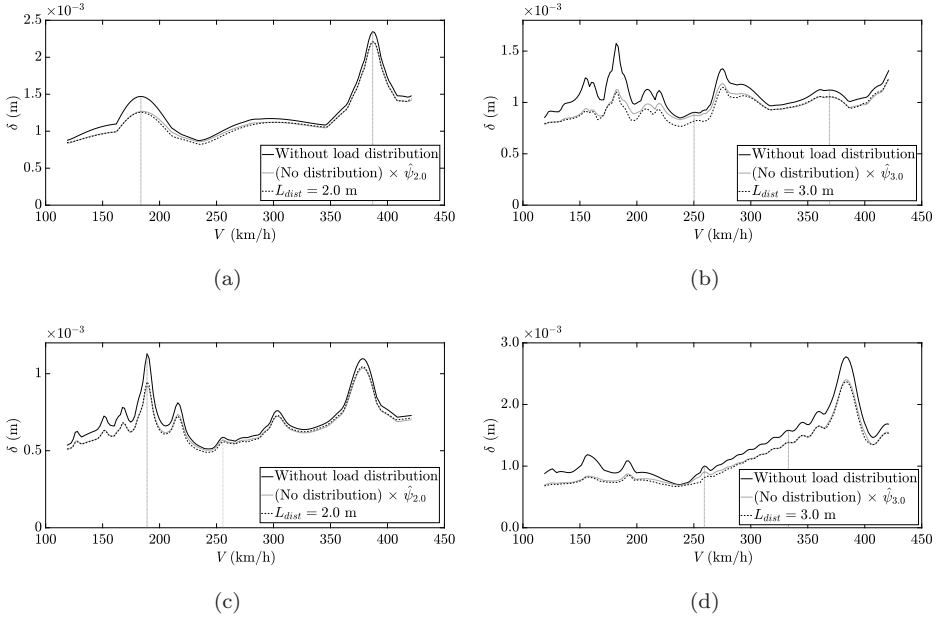
Fig. 16. Envelopes of vertical displacement for the bridge of 6.0 m span length considering different load intensities. (a) $L_{\text{dist}} = 2.0$ m with passage of Railjet, (b) $L_{\text{dist}} = 3.0$ m with Thalys (single), (c) $L_{\text{dist}} = 2.0$ m with Alfa Pendular, and (d) $L_{\text{dist}} = 3.0$ m with Renfe S-102 (single).

triangular load distribution and those obtained with the data-driven formula is very good.

In the above discussions, bridges with spans of less than 25.2 m were considered. This choice is mainly supported by the fact that the wavelength in longer bridges is often greater than 6.8 m, leading the load distribution within the track to result in negligible reductions in displacement responses. Despite this fact and for the sake of completeness, an additional bridge with a span length of 30.0 m is now considered to assess the performance of the proposed relationship for bridges with larger span lengths. The considered bridge has a fundamental frequency $f_1 = 4.138$ Hz, a linear mass of $m = 26\,205$ kg/m and a damping ratio of $\zeta = 1.0\%$. For comparison, the envelope curves of the vertical displacement of this bridge without load distribution, plus using the proposed relationship, and also with triangular load distribution with distributive length of 3.0 m, are compared under the action of Alfa Pendular and ICE-4 trains in Figs. 17(a) and 17(b). These two real trains are the ones that produce the highest positive and negative differences.

The results in Figs. 17(a) and 17(b) confirm the negligible reduction of displacement responses of bridges with larger spans due to the load distribution within the track. Moreover, the maximum positive and negative differences between the estimated responses using the proposed relationship and those from the triangular
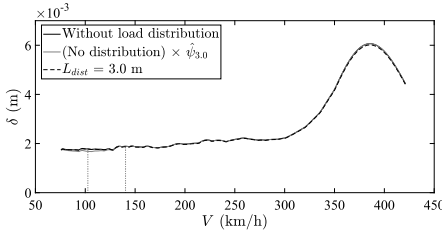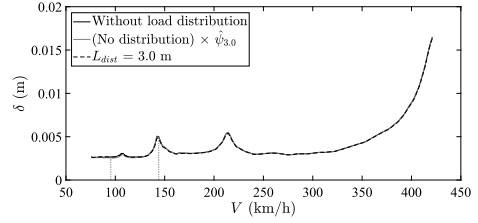
(a) $L_{\text{dist}} = 3.0\,\text{m}$ with Alfa Pendular.　　　(b) $L_{\text{dist}} = 3.0$ m with ICE-4.

Fig. 17. Envelopes of vertical displacement for the bridge of 30.0 m span length considering different load intensities.

load distribution within the track were $+5.28\%$ and -2.95%, respectively. The latter validates the suitable performance of the proposed relationship for predicting reduction factors of displacement responses of longer bridges.

In summary, the promising capabilities of the new data-driven formulas, which use simple input parameters as the wavelength (λ) and the impact factor (δ/δ_s) have been demonstrated.

8. Conclusions

New straightforward data-driven relationships are proposed in this paper to implicitly account for the effects of load distribution within track on the experienced deflection of railway bridges. This objective is achieved by creating a comprehensive dataset that includes simply-supported single-span bridges with span lengths of $[4.8-25.2]$ m under the passage of normative (articulated), conventional and regular trains with a wide range of operating speeds up to $420\,\text{km/h}$. The proposed relationships depend on only two input parameters, namely the wavelength and the impact factor.

To include the effects of tracks with different ballast depths in the proposed relationships, three distributive lengths corresponding to the conventional triangular distribution approach are considered. These distributive lengths comprise $L_{\text{dist}} = [2.0, 2.5, 3.0]\,\text{m}$ and essentially cover the lower, intermediate and upper practical limits of the distributive lengths.

The relationship for intermediate distributive lengths (i.e. $L_{\text{dist}} = 2.5\,\text{m}$) is based on a slight modification of a formula previously proposed by the authors. The mentioned modification adjusts the existing relationship for wavelengths shorter than 2.8 m. Subsequently, quadratic polynomial mapping functions are trained to transfer the reduction factor for the other considered distributive lengths.

The applicability of the proposed relationships is validated using both a test set extracted from the original dataset, and dynamic analyses of the bridges when subjected to the passage of 10 real trains. It should be noted that the latter trains

include also articulated, conventional and regular vehicles, that were not included in the training dataset. The validations performed showed the satisfactory accuracy of the proposed formulas. Based on these investigations, the maximum difference between the predicted reduction factor and the true values was below 10% in the majority of cases, while only in few situations the results delivered were slightly more conservative.

In 2002, UIC Leaflet 776-2R presented multiplicative factors that have been successfully applied to predict the reduction of the vertical acceleration in railway bridges due to the load spreading effect of ballasted tracks. The new relationships proposed in this paper constitute a simple and effective means to implicitly take into account such influence of the track in the predicted vertical displacements, without the need to create complex computational models. This can lead to considerable savings in computational budgets for situations requiring numerous dynamic assessments, including preliminary assessments, probabilistic investigations and sensitivity/screening analyses.

In the future, the proposed relationship is expected to be tested for other vehicle types (probably more of a theoretical nature), by the authors and other researchers — including "normative" load models from various countries. The further testing of the relationship for additional rolling stock configurations is therefore an ongoing work for the future. It should however be emphasized that in this investigation the formula has been [trained] + [tested] for a total of [1 251] (including 169 246 data point for each load distribution length) + [1 251 (including 72 531 data point for each load distribution length) + 10] train configurations, comprising conventional, articulated and regular vehicles. Regarding the type of bridge supports, currently the formula has been verified extensively for simply-supported spans, and other configurations will be investigated in the future.

Acknowledgments

ORCID

Reza Allahvirdizadeh ● https://orcid.org/0000-0002-8453-8937

Emma Moliner ● https://orcid.org/0000-0002-8142-1936

Pedro Museros ● https://orcid.org/0000-0002-1389-0204

References

1. IEA, Net Zero by 2050: A roadmap for the global enery sector, International Energy Agency (2021).
2. EEA, EEA Report No 19/2020: Transport and environment report. Train or plane? European Environment Agency (2020).
3. European Comission, COM(2020) 789 final. Sustainable and smart mobility strategy — putting European transport on track for the future (2020).
4. ERA, ERA1193-TD-01-2022 - ERA technical note on work needed for closing TSI open points on bridge dynamics, European Union Agency for Railways (2022).
5. EN 1990-2023/A2, Eurocode: Basis of structural design Annex A2, application for bridges, European Committee for Standardisation (CEN) (2023).
6. P. Montenegro, H. Carvalho, D. Ribeiro, R. Calçada, M. Tokunaga, M. Tanabe and W. Zhai, Assessment of train running safety on bridges: A literature review, *Eng. Struct.* **241** (2021) 112425.
7. J. Rocha, A. Henriques and R. Calçada, Probabilistic safety assessment of a short span high-speed railway bridge, *Eng. Struct.* **71** (2014) 99–111.
8. H. Yu, B. Wang, Y. Li and Z. Gao, A two-step framework for stochastic dynamic analysis of uncertain vehicle-bridge system subjected to random track irregularity, *Comput. Struct.* **253** (2021) 106583.
9. R. Allahvirdizadeh, A. Andersson and R. Karoumi, Improved dynamic design method of ballasted high-speed railway bridges using surrogate-assisted reliability-based design optimization of dependent variables, *Reliab. Eng. Syst. Saf.* **238** (2023) 109406.
10. R. Allahvirdizadeh, A. Andersson and R. Karoumi, Partial safety factor calibration using surrogate models: An application for running safety of ballasted high-speed railway bridges, *Probabilistic Eng. Mech.* **75** (2024) 103569.
11. C. D. Stoura and E. G. Dimitrakopoulos, A Modified Bridge System method to characterize and decouple vehicle-bridge interaction, *Acta Mech.* **231** (2020) 3825–3845.
12. L. R. T. Melo, D. Ribeiro, R. Calçada and T. N. Bittencourt, Validation of a vertical train–track–bridge dynamic interaction model based on limited experimental data, *Struct. Infrastruct. Eng.* **16**(1) (2020) 181–201.
13. A. Zangeneh, C. Svedholm, A. Andersson, C. Pacoste and R. Karoumi, Identification of soil-structure interaction effect in a portal frame railway bridge through full-scale dynamic testing, *Eng. Struct.* **159** (2018) 299–309.
14. K. Matsuoka, A. Collina, C. Somaschini and M. Sogabe, Influence of local deck vibrations on the evaluation of the maximum acceleration of a steel-concrete composite bridge for a high-speed railway, *Eng. Struct.* **200** (2019) 109736.
15. H. Li, T. Wang and H. Yan, Dynamic analysis of coupled train and cracked bridge systems using multiscale finite element modeling, *Int. J. Struct. Stab. Dyn.* **24**(6) (2024) 2450057.
16. W. Guo, Y. Long, C. He, Y. Wang, Y. Zeng and J. Song, Off-line hybrid simulation method on train–track–bridge coupling vibration in high-speed railway, *Int. J. Struct. Stab. Dyn.* **22**(10) (2022) 2241014.

17. A. Armijo and D. Zamora-Sánchez, Integration of railway bridge structural health monitoring into the internet of things with a digital twin: A case study, *Sensors* **24**(7) (2024) 2115.

18. S. Anastasia, E. García-Macías, F. Ubertini, V. Gattulli and S. Ivorra, Damage identification of railway bridges through temporal autoregressive modeling, *Sensors* **23**(21) (2023) 8830.

19. C. Wang, J. Zhan, Y. Wang, F. Zhang and D. Pan, A drive-by methodology for rapid inspection of hsr bridge substructures using dynamic responses of passing marshaling trains, *Int. J. Struct. Stab. Dyn.* **24**(6) (2023) 2450068.

20. R. Allahvirdizadeh, Improving the dynamic design philosophy of high-speed railway bridges using reliability-based methods, PhD thesis, KTH Royal Institute of Technology (2024).

21. C. Johansson, N. Nualláin, C. Pacoste and A. Andersson, A methodology for the preliminary assessment of existing railway bridges for high-speed traffic, *Eng. Struct.* **58** (2014) 25–35.

22. G. Grunert, Data and evaluation model for the description of the staticdynamic interface between trains and railway bridges, *Eng. Struct.* **262** (2022) 114335.

23. P. Museros, A. Andersson, V. Martí and R. Karoumi, Dynamic behaviour of bridges under critical articulated trains: Signature and bogie factor applied to the review of some regulations included in en 1991-2, *Proc. Inst. Mech. Eng. F* **235**(5) (2021) 655–675.

24. G. Ferreira, P. Montenegro, J. Pinto, A. A. Henriques and R. Calçada, A discussion about the limitations of the eurocode's high-speed load model for railway bridges, *Railw. Eng. Sci.* **32** (2024) 211–228.

25. M. Reiterer, M. Kwapisz, A. Firus, M. Rupp and G. Lombaert, Development of a new high-speed train load model for dynamic calculation of railway bridges, *ce/papers* **6**(5) (2023) 422–429.

26. A. Di Matteo, Dynamic response of beams excited by moving oscillators: Approximate analytical solutions for general boundary conditions, *Comput. Struct.* **280** (2023) 106989.

27. A. K. Rahman, B. Imam and D. Hajializadeh, Dynamic amplification of railway bridges under varying wagon pass frequencies, *Infrastructures* **9**(3) (2024) 62.

28. P. Museros, M. Romero, A. Poy and E. Alarcón, Advances in the analysis of short span railway bridges for high-speed lines, *Comput. Struct.* **80**(27) (2002) 2121–2132.

29. B. Glatz and J. Fink, Einfluss der zugmodelle auf die dynamische antwort von 75 stahl-, verbund- und stahlbetonbrücken, *Stahlbau* **88** (2019) 470–477.

30. EN 1991-2:2024, Eurocode 1: Actions on structures. Part 2: Traffic loads on bridges and other civil engineering works, European Committee for Standardisation (CEN) (2023).

31. ERRI, Rail bridges for speeds > 200 km/h. Final report (RP9), European Rail Research Institute (D-214 Committee, ERRI D-214) (1999).

32. UIC, Design requirements for rail-bridges based on interaction phenomena between train, track and bridge (UIC Code 776-2R), International Union of Railways (2009).

33. K. Kurrer, *The History of the Theory of Structures: From Arch Analysis to Computational Mechanics* (Ernst & Sohn, 2008).

34. A. Doménech, P. Museros and M. Martínez-Rodrigo, Influence of the vehicle model on the prediction of the maximum bending response of simply-supported bridges under high-speed railway traffic, *Eng. Struct.* **72** (2014) 123–139.

35. T. Arvidsson and R. Karoumi, Train-bridge interaction — A review and discussion of key model parameters, *Int. J. Rail Transp.* **2**(3) (2014) 147–186.

36. A. M. Kohl, K.-D. Clement, J. Schneider, A. Firus and G. Lombaert, An investigation of dynamic vehicle-bridge interaction effects based on a comprehensive set of trains and bridges, *Eng. Struct.* **279** (2023) 115555.

37. E. Axelsson, A. Syk, M. Ülker-Kaustell and J. Battini, Effect of axle load spreading and support stiffness on the dynamic response of short span railway bridges, *Struct. Eng. Int.* **24**(4) (2014) 457–465.

38. Z. Jin, B. Huang, J. Ren and S. Pei, Reduction of vehicle-induced vibration of railway bridges due to distribution of axle loads through track, *Shock Vib.* **2018** (2018) 2431980.

39. E. Moliner, P. Museros and R. Allahvirdizadeh, Track-bridge interaction effects in the acceleration and displacement response of highspeed railway bridges: simplified vs. refined modelling, *Eng. Struct.* **314** (2024) 118304.

40. A. Pesterev, B. Yang, L. Bergman and C. Tan, Revisiting the moving load problem, *J. Sound Vib.* **261** (2003) 75–91.

41. P. Museros, A. Andersson and B. Pinazo, Dynamic behaviour of bridges under critical conventional and regular trains: Review of some regulations included in EN 1991-2, *Proc. Inst. Mech. Eng. F*, *J. Rail Rapid Transit* **238**(8) (2024) 977–988.

42. P. Museros, A. Andersson and B. Pinazo, High-speed trains derived from Annex E/EN 1991-2, Mendeley Data (2023), doi:10.17632/hdr6dd5xv2.3.

43. ERRI D214.2, Use of universal trains for the dynamic design of railway bridges. Summary of results of D-214.2., European Rail Research Institute (D-214.2 Committee, ERRI D-214.2) (2002).

44. A. Firus, H. Berthold, J. Schneider and G. Grunert, Untersuchungen zum dynamischen verhalten einer eisenbahnbrücke bei anregung durch den neuen ice 4, *VDI-Berichte* **2321** (2018) 233–248.

45. J. Shu, Z. Zhang, I. Gonzalez and R. Karoumi, The application of a damage detection method using artificial neural network and train-induced vibrations on a simplified railway bridge model, *Eng. Struct.* **52** (2013) 408–421.

46. N. Zhang, H. Xia and W. Guo, Vehicle—bridge interaction analysis under high-speed trains, *J. Sound Vib.* **309**(3) (2008) 407–425.

47. G. Saramago, P. A. Montenegro, D. Ribeiro, A. Silva, S. Santos and R. Calçada, Experimental validation of a double-deck track-bridge system under railway traffic, *Sustainability* **14**(10) (2022) 5794.

48. G. Kouroussis, O. Verlinden and C. Conti, Free field vibrations caused by high-speed lines: Measurement and time domain simulation, *Soil Dyn. Earthq. Eng.* **31**(4) (2011) 692–707.

49. P. Galvín, A. Romero, E. Moliner, G. De Roeck and M. Martínez-Rodrigo, On the dynamic characterisation of railway bridges through experimental testing, *Eng. Struct.* **226** (2021) 111261.